IMPACT OF STEEL-CONCRETE SLIPPAGE ON CFST COLUMN LOAD CAPACITY UNDER COMPLEX LOADING CONDITIONS

Pham My[1]*, Dinh Ngoc Hieu[1,2], Le Khanh Toan[1], Dang Cong Thuat[1]

[1]The University of Danang - University of Science and Technology, Vietnam
[2]School of Architecture, Soongsil University, South Korea

*Corresponding author: pmy@dut.udn.vn

(Received: September 26, 2024; Revised: October 11, 2024; Accepted: October 12, 2024)

DOI: 10.31130/ud-jst.2024.524E

Abstract - Concrete-Filled Steel Tubular (CFST) columns are composite structures consisting of a steel tube and a concrete core, offering high load-bearing capacity, especially under complex loading conditions. When CFST columns are subjected to simultaneous compression, bending and torsion, the interaction between the concrete core and the steel tube plays a crucial role in the distribution of stress and deformation. A key factor that needs to be assessed is the relative slippage between the steel tube and the concrete core, as it directly impacts the load-bearing capacity and stability of the column. This study shows that when compression/bending and torsion are applied simultaneously, the bond between the concrete core and steel tube may weaken, leading to slippage, which in turn reduces the structural system's load-bearing efficiency. Understanding and accurately assessing the impact of this slippage is essential for improving design, ensuring CFST columns achieve optimal load-bearing performance in practice.

Key words - CFST; Combined compression-bending-torsion load; Torsional bearing capacity; Compressive torsional capacity; Numerical analysis.

1. Introduction

CFST columns are widely recognized for their superior load-bearing capacity and structural efficiency, combining the strength of steel with the compressive capacity of concrete. These columns are extensively used in high-rise, industrial buildings, industrial buildings, bridges, offshore structures, and other applications subjected to complex loading conditions [1-6]. Many previous studies have focused on the behavior of CFST columns under pure compression [7-9] and combined compression and bending [10-13]. However, in practice, one of the critical scenarios in structural engineering is the simultaneous application of torsion and compression [2-6, 14], which poses significant challenges to the performance of CFST columns.

In CFST columns under combined torsion and compression, the steel tube and concrete core interact crucially, affecting load distribution and failure mechanisms. The tube confines the concrete, boosting its strength, while the concrete prevents tube buckling. However, combined loads, particularly torsion, complicate this interaction, causing potential slippage between the tube and core, which reduces stiffness and load capacity.

Understanding CFST columns under simultaneous torsion and compression is crucial for enhancing design methods and ensuring structural safety. This paper explores how these loading conditions affect CFST columns, focusing on steel-concrete interaction, slippage, and its impact on overall performance using numerical methods.

2. Problem statement

A finite element analysis model examines the impact of relative slippage between the steel tube and concrete core on CFST columns' load-bearing capacity, comparing circular (Ci) and square (Sq) cross-sections as shown in Table 1 and Table 2. The analysis reveals how different slippage characteristics influence their ability to resist combined torsion, compression, and bending, helping assess the impact of slippage on CFST structures' load-bearing capacity.

The paper also includes parameter studies to determine critical torsional strength and moment for torsion-deformation curves in composite cross-sections. These results will support the development of theoretical models and improvements in design methods, enhancing safety and reliability for CFST structures under complex load combinations like compression-torsion, bending-torsion, and compression-bending-torsion.

3. Numerical model

3.1. Geometric and mechanical properties

The paper focuses on parameter studies by investigating changes in the geometry of the structural elements, variations in the material strength of the steel tube and concrete core, the ratio of compressive force to critical compressive force, or the ratio of bending moment to torsional moment, etc. Detailed information on the survey samples in the case of columns under combined compression and torsion is provided in Table 1, where n represents the level of axial force influence in the column and is defined as $n = N_k/N_u$, with N_k being the axial force applied to the column at the time of the survey, and N_u being the critical axial compressive force that the column can withstand.

In the case of CFST columns subjected to combined bending and torsion, the relative slippage between the steel tube and the concrete core is also predicted through finite element analysis. The evaluation results are compared between 9 simulations for circular cross-sections and 9 simulations for square cross-sections. Detailed information on the survey model for columns under combined bending and torsion is provided in Table 2, where $m_0 = M/T$ is the ratio of the bending moment to the torsional moment during the loading process.

In the case of CFST columns subjected to combined bending, compression, and torsion, this study only

investigates the simplest scenario where the compressive force varies from $N_k = 10kN$ to $N_k = 60kN$, with each step increasing by $10kN$ and an eccentricity of $e = 300mm$. Meanwhile, the geometric and material parameters remain as specified in Table 1. The investigation of relative slippage between the steel tube and the concrete core is still based on a comparative evaluation of circular and rectangular cross-sections, as in the previous two cases. This allows identification of which combined loading conditions pose the greatest risk to the structural elements.

Table 1. *Geometric and mechanical properties of survey samples for circular and square cross-sections under combined torsion and compression*

No	Mark	Sample demensions	Yield strength of steel tube	Comp. strength of concrete core	Compressive force/ critical compressive force ratio
-	-	D× $t \times l$	f_y	f_c	$n = N_k/N_u$
-	-	[mm]	[MPa]	[MPa]	-
1	CFT-Ci/Sq-N_k-1	138 ×4.5×450	324.34	30.4	0÷ 0.9
2	CFT-Ci/Sq-N_k-2	125 ×3.3×450	324.34	30.4	0÷ 0.9
3	CFT-Ci/Sq-N_k-3	125 ×4.5×2000	324.34	30.4	0÷ 0.9
4	CFT-Ci/Sq-N_k-4	138×3×2000	280	21.9	0÷ 0.9
5	CFT-Ci/Sq-N_k-5	114×4.5×387	280	21.9	0÷ 0.9
6	CFT-Ci/Sq-N_k-6	114×4.5×800	280	21.9	0÷ 0.9
7	CFT-Ci/Sq-N_k-7	139.8×3.5×2000	348.2	38.2	0÷ 0.9
8	CFT-Ci/Sq-N_k-8	139.8×4×2000	348.2	38.2	0÷ 0.9
9	CFT-Ci/Sq-N_k-9	139.8×4.5×2000	348.2	38.2	0÷ 0.9

Table 2. *Geometric and mechanical properties of survey samples for circular and square cross-sections under combined torsion and bending*

No	Mark	Sample dimensions	Yield strength of steel tube	Comp. strength of concrete core	Bending moment/ torsion moment ratio
-	-	D× $t \times l$	f_y	f_c	$m_o = M/T$
-	-	[mm]	[MPa]	[MPa]	-
1	CFT-Ci/Sq-U_k-1	138 ×4.5×450	324.34	30.4	0÷ 2.4
2	CFT-Ci/Sq- U_k -2	125 ×3.3×450	324.34	30.4	0÷ 2.4
3	CFT-Ci/Sq- U_k -3	125 ×4.5×2000	324.34	30.4	0÷ 2.4
4	CFT-Ci/Sq- U_k -4	138×3×2000	280	21.9	0÷ 2.4
5	CFT-Ci/Sq- U_k -5	114×4.5×387	280	21.9	0÷ 2.4
6	CFT-Ci/Sq- U_k -6	114×4.5×800	280	21.9	0÷ 2.4
7	CFT-Ci/Sq- U_k -7	139.8×3.5×2000	348.2	38.2	0÷ 2.4
8	CFT-Ci/Sq- U_k -8	139.8×4×2000	348.2	38.2	0÷ 2.4
9	CFT-Ci/Sq- U_k -9	139.8×4.5×2000	348.2	38.2	0÷ 2.4

3.2. Material models

3.2.1. Concrete

The Concrete Plastic Damage (CPD) model in ABAQUS simulates the behavior of concrete in CFST structures, predicting both tensile and compressive responses under confined lateral pressure [15, 16]. The yield function is based on effective hydrostatic pressure and equivalent Mises stress, influenced by integrated plastic strain rates for compression and tension. Users can adjust the plastic yield surface using K_c and σ_{b0}/σ_{c0}, which controls the shape of the deviatoric plane and the yield/compression stress ratio. A non-associated flow rule governs plastic strain increments, with the yield potential defined by the Drucker-Prager function. In this study, the concrete dilation angle is set between 15^0 and 18^0, with damage characterized by stiffness reduction upon unloading. Static loading allows for damage effects to be ignored. Numerical complexities are stabilized using a viscoplastic law, which aids convergence by introducing a small viscosity parameter. The uniaxial compressive stress-strain curve [17] is derived from standard tests, assuming a perfectly plastic curve post-peak stress. The tensile stiffness model addresses cracking, assuming stress reduction to zero upon crack formation. Tensile strength f_{ct} follows DIN-1045-1 standards, with Poisson's ratio at 0.2 and the modulus of elasticity from Table 1 and Table 2.

3.2.2. Steel

An elastic-plastic model with the von Mises yield criterion is used to describe the material behavior of the steel tube. The stress-strain relationship obtained from uniaxial tensile tests has been applied to the steel material model [17]. The Poisson's ratio is set at 0.3, and the material properties of the steel are taken from Table 1 and Table 2.

3.3. Mesh generation

After defining the geometry and material properties, the concrete core is meshed using 8-node 3D-stress C3D8R elements, which feature reduced integration with a single integration point. This is also suitable for the steel tube with a relatively large thickness (see Table 1 and Table 2), as these elements provide accurate stress-strain relationships and physical behavior modeling. Further, C3D8R elements use reduced integration to address shear locking issues and maintain high accuracy at integration points located at the element center. This approach requires smaller elements to capture stress concentrations at corners and edges effectively.

Reduced integration elements can exhibit hourglassing modes, but these are rare and do not typically affect well-defined meshes. When hourglassing does occur, it can impede convergence, but a properly generated mesh can mitigate this issue. These elements are preferred for complex stress states due to their reduced susceptibility to shear locking.

For shoulder column applications, absolute rigid elements are used. These elements are defined by a reference node, with their shape determined by rotating or translating a 2D profile or generating a mesh. Although the shape remains constant, the solid can move significantly. The mass and inertia are either calculated from the element distribution or assigned directly.

Motion for absolute rigid solids is controlled by boundary conditions on the reference node. Loads can be applied as concentrated or distributed loads on nodes or elements, or directly on the reference node. Absolute solids interact with the model through connections to deformation elements and contact with them.

3.4. Boundary conditions

The steel tube and concrete core at the base are fixed to a rigid steel plate controlled by a reference node. The

column is treated as having a fixed base, with the node constrained in all six displacement degrees of freedom. The study focuses on the column's critical behavior, applying a static load with displacement control at the top.

4. Results and discussion

4.1. Investigation of CFST columns subjected to simultaneous bending, compression and torsion

First, the paper focuses on discussing the typical curve of the torsional moment (resulting in shear stress) versus the angle of twist, as analyzed and calculated in Figure 1. Generally, the results show that to analyze the physical behavior of CFST columns under simultaneous compression and torsion, we can divide the relationship between the torsional moment and the angle of twist into three stages.

The first stage, OA, from the origin O to point A, is linear, indicating an elastic phase. Here, steel and concrete interact, with forces on the steel tube being transferred to the concrete core. At point A, slippage between the steel tube and concrete core begins, and steel yielding starts.

In the second stage, from point A to point B, the curve transitions from a straight line (OA) to a nonlinear curve (AB). Simulations reveal slippage between the concrete core and steel tube, indicating nonlinear elastic-plastic behavior. During this phase, increasing torque causes concrete cracking and lateral expansion. The steel tube restricts this expansion, with resistance growing due to friction as torsion increases. This continues until reaching point B.

In the third stage, shown as segment BC on the graph, rapid slippage occurs due to cracks in the concrete core, causing partial core failure. The steel tube now predominantly supports the load, making the BC curve slope nearly horizontal. This results in significant deformation and strain hardening of the steel tube. Consequently, torque increases very slowly, making this stage known as the "reinforcement stage".

Figure 1-a compares the performance of CFST column components: the red line shows the torque-rotation relationship for the CFST column, the navy blue line for a steel-only column, and the green line for a concrete-only column. The results indicate that individual components are significantly less effective than the combined CFST structure, with the steel tube being vital for the column's torsional strength.

Figure 1-b shows the physical behavior of a CFST column with a square cross-section, revealing differences compared to circular cross-sections. This comparison underscores the critical impact of slippage and offers engineers insights for developing effective design solutions to improve structural performance.

Analysis reveals that slippage reduces the CFST column's load-bearing capacity instantly, as the load distribution between the steel tube and concrete core becomes ineffective. The steel tube then bears most of the load, rapidly moving from plastic deformation to strain hardening. Thus, an effective anti-slippage mechanism between the steel tube and concrete core is crucial to improve the structure's load-bearing capacity.

Comparing Figure 1-a,b reveals that slippage occurs later in CFST columns with a square cross-section. The torque at point A, where it becomes critical during the elastic stage, is higher for the square cross-section (52.7 kN.m) than for the circular cross-section (29.6 kN.m). This means the square cross-section extends the elastic range further due to more difficult slippage, leading to better interaction between the concrete core and the steel tube and increased overall stiffness.

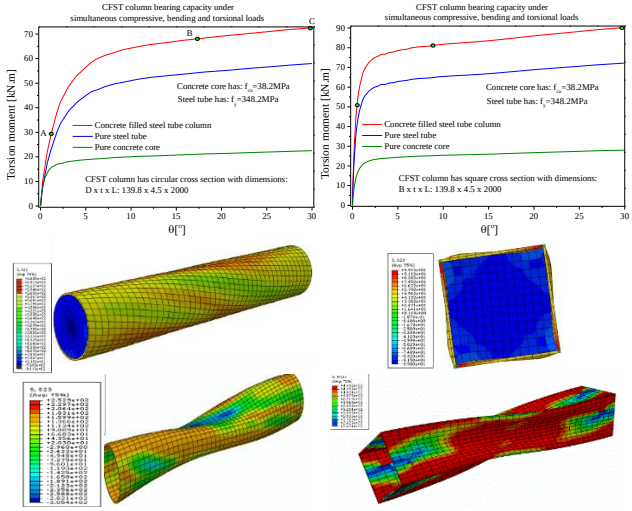

a) Circular CFST columns *b) Circular CFST columns*

Figure 1. *Relationship between shear stress and rotation angle for CFST columns, pure concrete core and steel tube*

At point B, the CFST column with a square cross-section is closer to the origin and has a shorter elastic-plastic range than the circular cross-section column. The torque at point B is higher for the square cross-section (79.4 kN.m) compared to the circular cross-section (68.2 kN.m). This is due to the combined geometric and material nonlinearities in the AB stage. The circular cross-section experiences premature slippage, leading to more stress redistribution and strain hardening at a greater distance from the origin. In contrast, the square cross-section distributes the load more efficiently and reaches point B due to concrete failure before the steel reaches strain hardening. When concrete fails, the load quickly shifts to the steel, causing rapid strain hardening. In Stage 3, both cross-sectional types show similar behavior due to the steel tube's dominant role.

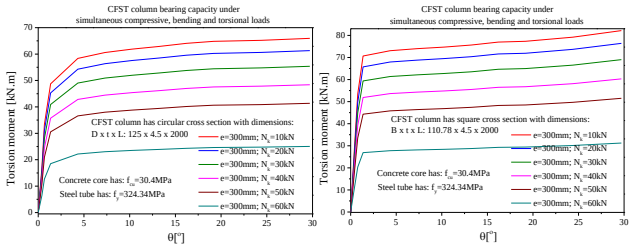

a) Circular CFST columns (D=125 mm) *b) Square CFST columns (B=110.78 mm)*

Figure 2. *Investigate the relationship between rotation angle and torque for CFT-Ci/Sq- U_k -3 model*

Figure 2-a,b depict the $(T-\theta)$ curves for a column with an axial load N_k applied at an eccentricity of $e = 300mm$ from the centroid. This setup simulates combined bending, compression, and torsion. The analysis increments N_k from

10kN to 60kN in 10kN steps, revealing a decreasing $(T-\theta)$ relationship. At N_k of 40kN, the column's torsional resistance drops sharply. The results illustrate how increasing bending moments and axial loads generate shear stresses that reduce both shear and torsional resistance.

We compare the circular column (Figure 2-a) and the square column (Figure 2-b) at a 15° rotation angle with an axial load of $N_k = 10kN$. The circular column has a diameter of $D = 125mm$, a steel tube thickness of $t = 4.5mm$, a length of $l = 2000mm$, a steel yield strength of $f_y = 324.24MPa$, and a concrete compressive strength of $f_{cu} = 30.4MPa$. The square column has a side length of $B = 110.78mm$, with other properties identical to the circular column. The torques are 62.8 kN.m for the circular column and 75.4 kN.m for the square column. Thus, the square column fails earlier and exhibits 16.72% higher torque at a 15° rotation angle compared to the circular column.

For CFST columns under complex loading (bending, compression, and torsion), increasing the eccentric axial load reduces torsional resistance. Additionally, square cross-sections fail earlier than circular ones.

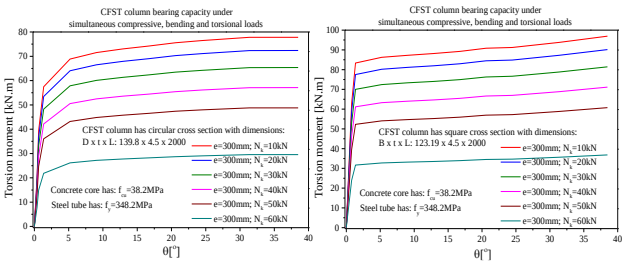

a) Circular CFST columns (D=139.8 mm) *b) Square CFST columns (B=123.19 mm)*

Figure 3. *Investigate the relationship between rotation angle and torque for CFT-Ci/Sq- U_k -9 model*

The study proceeds under the same conditions as in Figure 3-a,b, but with changes in the columns' geometry and mechanical properties. For the circular column, the diameter is $D = 139.8mm$, steel thickness $t = 4.5mm$, length $l = 2000mm$, yield strength $f_y = 348.2MPa$, and concrete compressive strength $f_{cu} = 38.2MPa$. For the square column, the side length is $B = 123.19mm$, with other parameters the same. Compared to Figure 2-a,b, the column size increases by 10.59%, steel yield by 6.85%, and concrete strength by 20.42%. Torque at $N_k = 10kN$ and 200° rotation shows a 14.9% increase for the circular and 16.25% for the square column. Thus, with increased parameters, the square column fails sooner.

4.2. Investigation of CFST columns subjected to simultaneous compression and torsion

Figure 4-a,b analyze the load-bearing capacity through the torque-rotation relationship, varying the axial load influence $(n = N_k/N_u)$. The study uses these parameters: circular column $(D = 114mm,\ t = 4.5mm,\ l = 1200mm, f_y = 280MPa, f_{cu} = 21{,}9MPa)$ and square column $(B = 101.03mm$, with identical other properties). As n increases from 0.2 to 0.8 in 0.2 increments, torsional resistance decreases. From Figure 7-a, when $n \geq 0.5$, CFST columns' torque resistance drops rapidly. Thus, increasing axial load reduces torsional resistance.

Comparing Figure 4-a,b and Figure 7-a reveals that the square cross-section column reaches the ultimate torque faster than the circular one, highlighting the importance of slippage between the steel tube and concrete core in torsional resistance. At a rotation angle of 15^0 and $n = 0.2$, the circular column's torque is 35.2 kN.m, while the square column's is 49.8 kN.m, meaning the square column reaches the ultimate value 29.32% sooner.

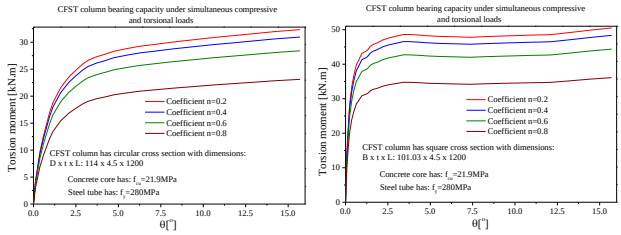

a) Circular CFST columns (D=114 mm) *b) Square CFST columns (B=101.03 mm)*

Figure 4. *Investigate the relationship between rotation angle and torque for CFT-Ci/Sq-N_k-6 model*

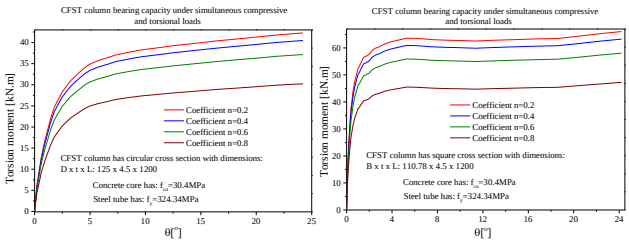

a) Circular CFST columns (D=125 mm) *b) Square CFST columns (B=110.78 mm)*

Figure 5. *Investigate the relationship between rotation angle and torque for CFT-Ci/Sq-N_k-2 model*

Figure 5-a,b and Figure 7-b compares the torsional capacity of CFST columns with circular and square cross-sections, using modified geometric and mechanical properties. For the circular column, $D = 125mm$, $t = 4.5mm$, $l = 1200mm$, $f_y = 324.24MPa$, and $f_{cu} = 34.24MPa$; for the square column, B = 110.78mm, with other parameters unchanged. The behavior mirrors that in Figure 4-a,b and Figure 7-a. At a rotation angle of 15^0 and $n = 0.2$, increasing column size by 8.8%, steel yield by 13.6%, and concrete strength by 36.04% raises torque by 9.51% for the circular column and 21.45% for the square. The square column's torque surpasses the circular by 11.94%.

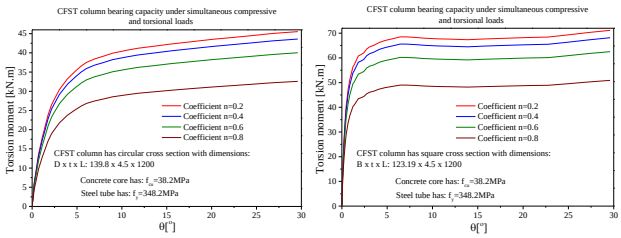

a) Circular CFST columns (D=139.8 mm) *b) Square CFST columns (B=123.19 mm)*

Figure 6. *Investigate the relationship between rotation angle and torque for CFT-Ci/Sq-N_k-9 model*

Figure 6-a,b and Figure 7-c assess the torsional capacity of CFST columns with circular and square cross-sections using different geometric and mechanical properties: For the circular column, the diameter is 139.8mm, tube thickness is 4.5mm, length is 1200mm, steel yield strength

is 348.2MPa, and concrete compressive strength is 38.2MPa. For the square column, the side length is 123.89mm, with other parameters identical to the circular column. The behavior aligns with the results in Figure 4-a,b and Figure 7-a.

We analyze a typical case at a 15^0 rotation angle and an axial load influence factor of $n = 0.2$. Increasing the column diameter by 18.45%, steel yield strength by 19.59%, and concrete compressive strength by 42.67% results in a 18.52% increase in torque for the circular column and a 46.83% increase for the square column. This confirms that with equivalent size and material property increments, the square column's torque increases by 28.31% more than the circular column.

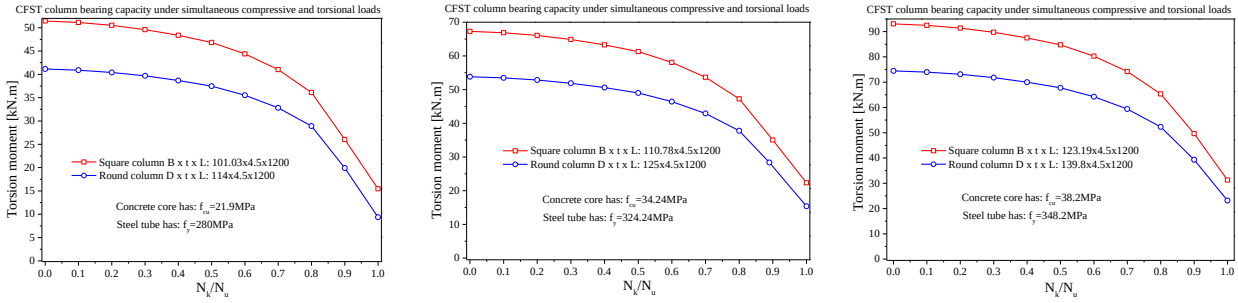

a) Column 114×4.5×1200mm *b) Column 125×4.5×1200mm* *c) Column 139.8×4.5×1200mm*

Figure 7. *Comparison of load-bearing capacity between circular and square columns under combined compression and torsion*

Figure 8-a,b assess how torque affects the strain-axial compressive force relationship in the steel tube shell. For the circular column, while the axial load initially increases rapidly, strain in the steel tube rises slowly because the concrete core shares some of the stress. As sliding begins, the core transfers less stress to the steel tube, causing strain to increase rapidly. This leads to plastic deformation in the steel tube, marked by a yield plateau on the $N - \varepsilon$ curve. As the axial load approaches the column's critical compressive force, the steel tube reaches its ultimate strength. Eventually, the tube loses its load-bearing capacity, and although the load decreases, column strain continues to rise.

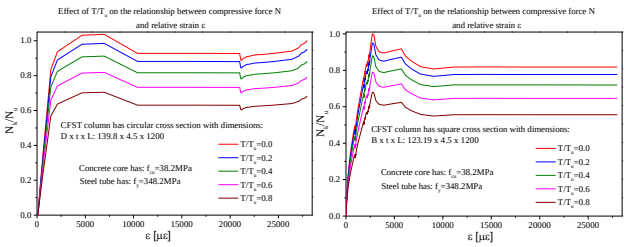

a) Circular CFST columns *b) Square CFST columns*

Figure 8. *Examine the correlation between axial force and relative deformation*

In the square column, sliding is more difficult, so the concrete core continuously shares stress with the steel tube, causing strain in the tube to increase slowly until the axial load reaches the critical value. The column fails suddenly and brittlely due to the concrete core (see Figure 8-b), even though the steel tube has not reached its ultimate strength. The steel then bears most of the load, reaching its yield point before its strength value. Due to continuous cold hardening, the steel's strength at a strain of $7340(\mu\varepsilon)$ is lower than for the circular column. The column then loses load-bearing capacity, with axial load decreasing and strain increasing until complete failure.

Figure 8-a,b illustrate that increased torque reduces the axial compressive strength of the column. This occurs because torque accelerates slippage between the steel tube and the concrete core, thereby diminishing the column's axial load-bearing capacity.

4.3. Investigation of CFST columns subjected to simultaneous bending and torsion

This section investigates how bending moment affects the torsional resistance of columns with circular and square cross-sections, considering variations in geometric and mechanical parameters. Figure 9-a,b shows the relationship between torque and rotation angle under different bending moment impacts (M_k). For the circular column with $D = 114mm$, $t = 4.5mm$, $l = 1200mm$, $f_y = 280MPa$, and $f_{cu} = 21.9MPa$, and the square column with $B = 101.03mm$, similar trends are observed. The results, combined with Figure 12-a, reveal that increasing M_k decreases torsional resistance due to the additional shear forces generated by the bending moment, which, along with torque-induced shear forces, reduces the column's torsional strength.

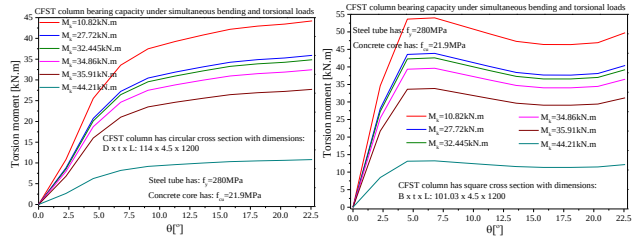

a) Circular CFST columns (D=114 mm) *b) Square CFST columns (B=101.03mm)*

Figure 9. *Analyze the correlation between rotation angle and torque for CFT-Ci/Sq- U_k -6 model*

Figure 9 to Figure 11-b reveals that bending moments shift the $T - \theta$ curve away from the OT axis more than axial loads (given in Figure 4 to Figure 6-b) which only causes volumetric expansion and increases friction between the steel tube and concrete core. This friction limits slippage and reduces rotation. In contrast, bending moments generate shear forces that ease slippage, increasing rotation and shifting the $T - \theta$ curve.

Comparing Figure 10-a,b, at a 5^0 rotation and $M_k = 14.15kN.m$, the circular column's torque is 27.5 kN.m, while the square column's torque approaches 70.2 kN.m. This shows the square column reaches failure

more quickly with a smaller rotation angle. The circular column requires 5-6 times the rotation angle to fail, indicating it has a better load-bearing capacity and more effective stress distribution than the square column. See Figure 16-a,b for details.

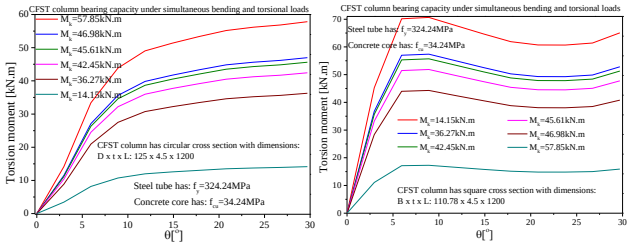

a) Circular CFST columns (D=125mm) *b) Square CFST columns (B=110.78mm)*

Figure 10. *Analyze the correlation between rotation angle and torque for CFT-Ci/Sq- U_k -3 model*

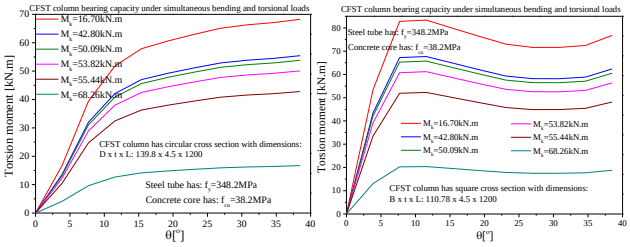

a) Circular CFST columns (D=125mm) *b) Square CFST columns (B=110.78mm)*

Figure 11. *Analyze the correlation between rotation angle and torque for CFT-Ci/Sq- U_k -3 model*

Figure 10-a,b align with Figure 11-a,b. This section compares in Figure 11-a,b and Figure 12-c by examining changes in geometric and mechanical parameters, and bending moment M_k, relative to Figure 9 and Figure 12-a. For the circular column ($D = 139.8mm$, $t = 4.5mm$, $l = 1200mm$, $f_y = 348.2MPa$, $f_{cu} = 38.2MPa$) and the square column ($B = 123.89mm$) with $M_k = 14.15kN.m$ at 10^0 rotation, increasing column diameter/size by 18.45%, steel yield strength by 19.59%, and concrete compressive strength by 42.67% results in torque increases of 18.52% for the circular column and 46.83% for the square column, with an overall torque rise of 35.2%.

At a rotation angle of $\theta = 10^0$, torque increases by 11.54% for the circular column and 38.44% for the square column. This shows that while geometric size and mechanical properties influence torque, the cross-sectional shape is the most significant factor. It highlights that relative slippage affects the torsional resistance of CFST columns.

Figure 12 shows that as the bending moment increases, the torque in CFST columns decreases and reaches zero when the bending moment hits the critical value for pure bending. Torque is highest when the bending moment is zero. The results indicate that, for varying mechanical properties and geometry, a square cross-section has a higher torque value compared to a circular one. This is because a circular column distributes stress more evenly, while a square column distributes it unevenly (as given in Figure 16-a,b). Consequently, within a small rotation angle, a square column reaches its critical torque value faster than a circular column, making the circular cross-section more effective for torsional resistance in CFST structures.

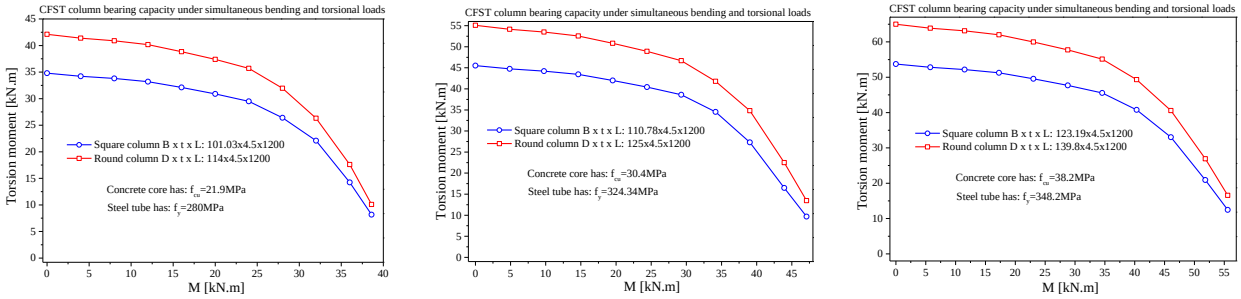

a) Column 114×4.5×1200mm *b) Column 125×4.5×1200mm* *c) Column 139.8×4.5×1200mm*

Figure 12. *Comparison of load-bearing capacity between circular and square columns under combined bending and torsion*

4.4. Investigation of steel tube-concrete core interaction and other behaviors of CFST columns

This section explores the physical impact of slippage on CFST column torsional resistance. We first analyze the relationship between confining stress, concrete lateral expansion, and rotation angle, as shown in Figure 14-a,b.

Before analyzing the results, we explain how the rotation angle is applied to the column top. This setup mimics real-world applications like utility poles, bridge piers, or corner columns in high-rise buildings subject to seismic loads. These structures experience rotation via beams attached to the top. The study simulates this by modeling the column as a rigid body with loads applied through a reference node, as shown in Figure 13.

Figure 14-a illustrates the relationship between rotation angle (θ) and confining stress (p) at two points, A and B. For small rotation angles, confining stress increases rapidly at both points. At point B, stress rises faster and reaches 5.84 MPa at $\theta = 0.82^0$, while at point A, the same stress level is achieved at $\theta = 2.24^0$. The stress at point B drops suddenly due to its position relative to the rotation angle, whereas point A's stress decrease is slower. Both points have the same confining stress value at failure. As noted in section 4.1, a circular column fails when the steel tube reaches its ultimate strength, resulting in a positive maximum confining stress.

For the square column, Figure 14-b shows similar initial behavior. However, after slippage and concrete core failure, the confining stress in the steel tube becomes negative.

At failure, the square column has a higher confining stress ($p = 12.3\,MPa$) compared to the circular column ($p = 5.84\,MPa$), due to the more restricted slippage in the square cross-section.

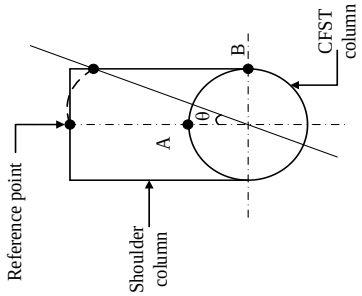

Figure 13. *CFST column top rotation mechanism*

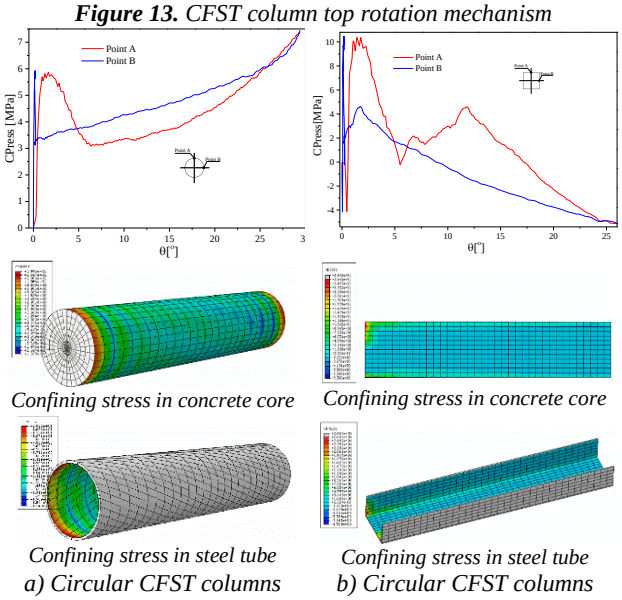

a) Circular CFST columns *b) Circular CFST columns*

Figure 14. *The relationship between confining stress on the concrete core and rotation angle for circular cross-sections*

Figure 15-a,b illustrate the relationship between confining stress and the steel tube's relative deformation. When the rigid plate rotates at a small angle (see Figure 13), confining stress at both points A and B rapidly escalates with deformation. Point A moves tangentially along the column perimeter, while point B presses toward the concrete core, causing B's stress to surge to 25 MPa with minimal deformation. Slippage then occurs, dropping and reversing the stress, but as the concrete core expands, the stress recovers, climbing to its critical point.

At point A in Figure 15-a, a larger deformation is needed before stress rises. Initially, it spikes, then briefly dips with minor slippage, but rebounds and climbs until further slippage causes another drop. Finally, a new equilibrium is reached, the stress rises again to 25 MPa, and major slippage at both points results in stress reversal. By this stage, most stress is concentrated in the deformed steel tube, driving contact pressure higher until the structure reaches its critical state, where stress at points A and B equalizes.

For the relationship between confining stress and deformation in the square column shown in Figure 15-b:

At points A and B, the deformation reaches the same state, corresponding to a confining stress of about 9.26 MPa. After this, slippage occurs, and the confining stress starts to decrease as the concrete expands. At point B, the stress drops rapidly, nearing zero, indicating that the steel tube and concrete core are no longer in contact. The stress then recovers until the steel tube's relative deformation reaches approximately 10867$\mu\varepsilon$, at which point the concrete core fails and the confining stress reduces to a critical state.

At point A, after slippage, the confining stress drops to around 1500 $\mu\varepsilon$, establishing a new equilibrium. The stress then increases again, while the concrete around point A cracks. The confining stress fluctuates until the relative deformation reaches 6040 $\mu\varepsilon$, at which point the concrete around point A fails, and the stress quickly drops to a critical state. At the critical state, the confining stress values at points A and B are equal.

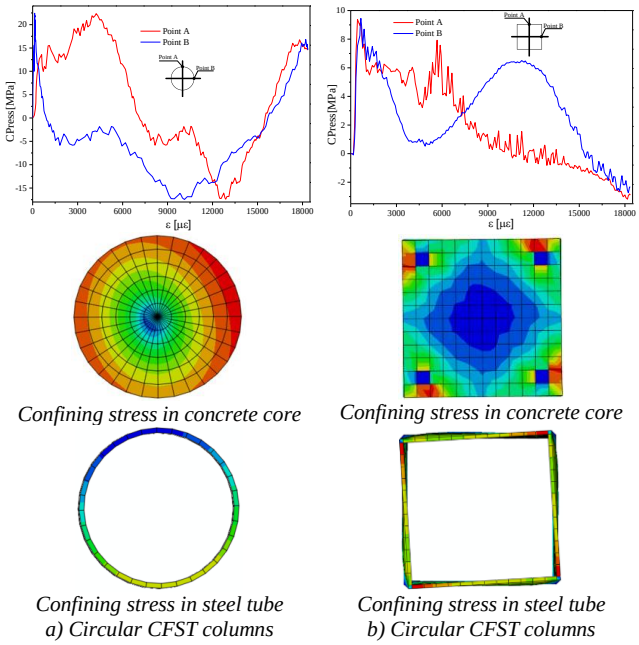

a) Circular CFST columns *b) Circular CFST columns*

Figure 15. *The relationship between confining stress on the concrete core and rotation angle for circular sections*

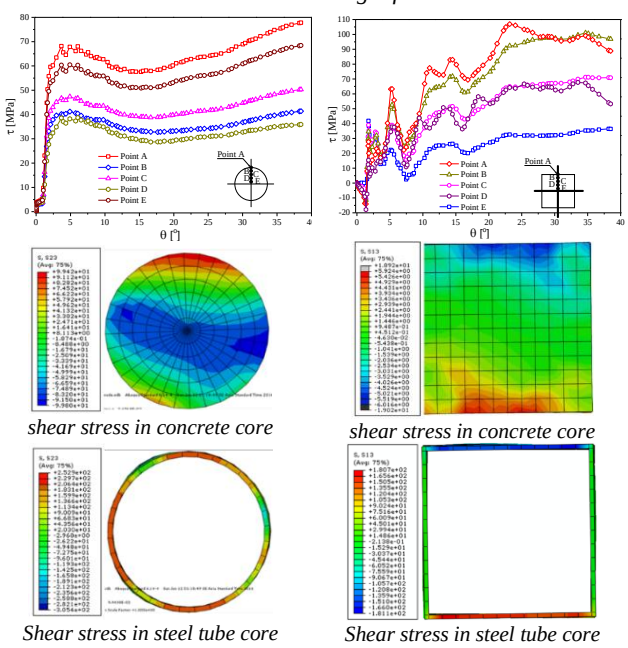

a) Circular CFST columns *b) Circular CFST columns*

Figure 16. *The relationship between shear stress and rotation angle at points A to E for circular cross-sections*

Figure 16-a,b shows the shear stress versus rotation angle at points A to E for circular and square columns.

Initially, shear stress rises rapidly, then increases more moderately during the elastic-plastic stage. For circular columns, shear stress is distributed from the center to the perimeter as loading progresses. The $\tau - \theta$ curve indicates that shear stress peaks between 2.5^0 and 7.5^0 rotation angles. Within this range, slippage between the steel tube and concrete core begins, reducing shear stress in the core as stress is not fully transferred. This leads to a new equilibrium, with continued slippage and increasing shear stress until column failure.

In square columns, shear stress rises rapidly initially, spreading from the center to the perimeter like in circular columns. However, the uneven shear stress distribution leads to earlier crack formation in the concrete core, increasing its volume and complicating the column's behavior.

In both square and circular columns, shear stress fluctuates due to the interaction between the steel tube and concrete core and the nonlinear material behavior. Despite these variations, shear stress generally increases until the column fails.

5. Conclusion

The paper reviews CFST columns under combined axial compression, torsion, and partial bending. Key findings include:

- Slippage between concrete core and steel tube reduces load-bearing capacity in both circular and square columns. Slippage occurs slower in square columns, extending their elastic range. For instance, slippage in circular columns (139.8 × 4.5 × 1200 mm) happens at 29.6 kN.m torque, while in square columns (123.19 × 4.5 × 1200 mm) it occurs at 52.7 kN.m. However, square columns reach failure earlier and bear more load than circular ones with equal cross-sectional areas.

- Under combined compression and torsion, higher axial force reduces torsional resistance and causes earlier slippage. Square columns have greater torsional resistance than circular ones as geometric and mechanical parameters increase. At a 15° rotation, a circular column (114 × 4.5 × 1200 mm) reaches 35.2 kN.m torque, while a square column (101.03 × 4.5 × 1200 mm) reaches 49.8 kN.m, a 29.32% increase.

- In combined bending and torsion, bending induces shear forces, reducing torsional resistance, with square columns failing sooner. At a 50° rotation, a square column's torsion moment (with 14.15 kN.m bending) is 70.2 kN.m, while a circular column has 27.5 kN.m.

- Slippage in square columns is more restricted, often resulting in negative values due to concrete failure, while circular columns show positive values. Confining stress at slippage is 12.3 MPa for square columns and 5.84 MPa for circular ones.

REFERENCES

[1] N. E. Shanmugam and B. Lakshmi, "State of the art report on steel–concrete composite columns", *Journal of Constructional Steel Research*, vol. 57, no. 10, pp. 1041-1080, 2001, doi: https://doi.org/10.1016/S0143-974X(01)00021-9.

[2] J.-g. Nie, Y.-h. Wang, and J.-s. Fan, "Experimental study on seismic behavior of concrete filled steel tube columns under pure torsion and compression–torsion cyclic load", *Journal of Constructional Steel Research*, vol. 79, pp. 115-126, 2012, doi: https://doi.org/10.1016/j.jcsr.2012.07.029.

[3] Q.-X. Ren, L.-H. Han, C. Hou, Z. Tao, and S. Li, "Concrete-encased CFST columns under combined compression and torsion: Experimental investigation", *Journal of Constructional Steel Research*, vol. 138, pp. 729-741, 2017, doi: https://doi.org/10.1016/j.jcsr.2017.08.016.

[4] W. Xing, Q. Shen, J. Wang, and M. Sheng, "Performance and design of oval-ended elliptical CFT columns under combined axial compression-torsion", *Journal of Constructional Steel Research*, vol. 172, p. 106148, 2020, doi: https://doi.org/10.1016/j.jcsr.2020.106148.

[5] Y.-H. Wang *et al.*, "Combined compression-bending-torsion behaviour of CFST columns confined by CFRP for marine structures", *Composite Structures*, vol. 242, p. 112181, 2020, doi: https://doi.org/10.1016/j.compstruct.2020.112181.

[6] Y.-H. Wang *et al.*, "Coupled ultimate capacity of CFRP confined concrete-filled steel tube columns under compression-bending-torsion load", *Structures*, vol. 31, pp. 558-575, 2021, doi: https://doi.org/10.1016/j.istruc.2021.01.086.

[7] L.-H. Han and Y.-F. An, "Performance of concrete-encased CFST stub columns under axial compression", *Journal of Constructional Steel Research*, vol. 93, pp. 62-76, 2014, doi: https://doi.org/10.1016/j.jcsr.2013.10.019.

[8] Q.-X. Ren, L.-H. Han, D. Lam, and C. Hou, "Experiments on special-shaped CFST stub columns under axial compression", *Journal of Constructional Steel Research*, vol. 98, pp. 123-133, 2014, doi: https://doi.org/10.1016/j.jcsr.2014.03.002.

[9] L. Xu, J. Pan, and X. Yang, "Mechanical performance of self-stressing CFST columns under uniaxial compression", *Journal of Building Engineering*, vol. 44, p. 103366, 2021, doi: https://doi.org/10.1016/j.jobe.2021.103366.

[10] Y.-F. An and L.-H. Han, "Behaviour of concrete-encased CFST columns under combined compression and bending", *Journal of Constructional Steel Research*, vol. 101, pp. 314-330, 2014, doi: https://doi.org/10.1016/j.jcsr.2014.06.002.

[11] Q.-X. Ren, L.-H. Han, C. Hou, and Y.-X. Hua, "Experimental behaviour of tapered CFST columns under combined compression and bending", *Journal of Constructional Steel Research*, vol. 128, pp. 39-52, 2017, doi: https://doi.org/10.1016/j.jcsr.2016.08.005.

[12] Y.-F. Yang and L.-H. Han, "Behaviour of concrete filled steel tubular (CFST) stub columns under eccentric partial compression", *Thin-Walled Structures*, vol. 49, no. 2, pp. 379-395, 2011/02/01/ 2011, doi: https://doi.org/10.1016/j.tws.2010.09.024.

[13] D. H. H. Phan, V. I. Patel, H. Al Abadi, and H.-T. Thai, "Analysis and design of eccentrically compressed ultra-high-strength slender CFST circular columns", *Structures*, vol. 27, pp. 2481-2499, 2020, doi: https://doi.org/10.1016/j.istruc.2020.08.037.

[14] R. Deng *et al.*, "Behaviour of tapered concrete-filled double-skin steel tubular columns with large hollow ratio under combined compression-bending-torsion loads: Experiments", *Journal of Building Engineering*, vol. 57, p. 104876, 2022, doi: https://doi.org/10.1016/j.jobe.2022.104876.

[15] J. Lubliner, J. Oliver, S. Oller, and E. Oñate, "A plastic-damage model for concrete", *International Journal of Solids and Structures*, vol. 25, no. 3, pp. 299-326, 1989, doi: https://doi.org/10.1016/0020-7683(89)90050-4.

[16] J. Lee and L. Fenves Gregory, "Plastic-Damage Model for Cyclic Loading of Concrete Structures", *Journal of Engineering Mechanics*, vol. 124, no. 8, pp. 892-900, 1998, doi: https://doi.org/10.1061/(ASCE)0733-9399(1998)124:8(892).

[17] L. X. Dung and P. My, "Investigation Into Relative Sliding Effect Between Steel Tube And Concrete Core On Eccentric Compression Resistance Of Concrete Filled Steel Tube Columns", *UD-JST*, vol. 1, no. 98, pp. 15-21, 2016, doi: https://jst-ud.vn/jst-ud/article/view/567.